Flow Characteristics in a Microchannel Condensers With Extraction Circuitry

Jun Li
ACRC, the University of Illinois, Urbana, Illinois, USA, junli9@illinois.edu

Vladimir Munćan
ACRC, the University of Illinois, Urbana, Illinois, USA

Dandong Wang
ACRC, the University of Illinois, Urbana, Illinois, USA

Pega Hrnjak
ACRC, the University of Illinois, Urbana, Illinois, USA

Flow Characteristics in a Microchannel Condensers With Extraction Circuitry

Jun Li[1], Vladimir Munćan[2], Dandong Wang[1], Pega Hrnjak[1,3]*

[1]ACRC, the University of Illinois, Urbana, Illinois, USA

[2]University of Novi Sad, Novi Sad, Serbia

[3]Creative Thermal Solutions, Inc., Urbana, Illinois, USA

* Corresponding Author, pega@illinois.edu

ABSTRACT

The present study reveals the characteristics of refrigerant flow in a microchannel condenser with the extraction circuitry. The extraction circuitry provides a potential to enhance the condenser performance at almost no cost – the condenser geometry is the same except for a few well-sized drainage holes in the header baffle. A microchannel condenser is modified to run in both the extraction mode and the conventional mode. A 1-D finite-volume model is built for the condenser and is validated with R134a experimental data. The capacities agree within ±5 % and the pressure drops agree within ± 25 %. Using this model, a numerical study is conducted on the condenser. A single-extraction-tube design and a double-extraction-tube design for the extraction mode are both simulated and compared. The flow characteristics in the extraction tube are revealed for a physically possible range of liquid separation efficiency. The effects of flow resistance in the extraction tube on the phase separation efficiency and the condenser performance are also studied.

1. INTRODUCTION

In a condensation process, liquid on the wall of the condenser is an extra thermal resistance reducing heat transfer. At the same mass flux, as condensate is formed from a high vapor quality ($x \sim 0.9$), the heat transfer coefficient (HTC) and the pressure gradient (dp/dz) generally decrease. Removing the liquid phase decreases dp/dz in the same flow passage or increases HTC for the same mass flux, so it can be a way to improve the condenser performance.

Microchannel condensers, mostly used in mobile air conditioners and recently in stationary systems, usually adopt the multi-pass design. For a microchannel condenser, two kinds of pass circuitries can remove liquid at low cost to improve the performance: separation and extraction. Separation refers to separating the liquid from vapor, then reassigning the flow passages for separated vapor and separated liquid. Details can be found in Li and Hrnjak (2017a; 2017b; 2021a; 2021b). The extraction of liquid in microchannel condensers can be designed as shown non-exhaustively in Figure 1, which only focuses on single-slab, parallel-tube, cross-flow microchannel condensers. Different from a conventional microchannel condenser, the extraction condenser is designed to extract liquid in the vertical intermediate headers through one or a few well-designed holes in the lower baffle directly to the exit of the condenser or to the passes further downstream. The liquid phase moves through the hole mainly due to the pressure difference. If the liquid can be drained efficiently, the flow rate in downstream passes will be lower, thus effectively reducing the pressure drop and elevating the refrigerant temperature. Besides, the flow at the inlet of the downstream pass is close to the onset of condensation, where the HTC is the highest. These factors may increase the heat transfer rate, i.e. the capacity, of the downstream passes.

In the literature, configurations for liquid extraction has been mostly applied to round-tube condensers, plate-type condensers, and shell-and-tube condensers (Wu et al., 2010; Ye et al., 2009; Chen et al., 2012; Luo et al., 2016; Chen et al., 2019; Zhang et al., 2019; Li et al., 2019). The present study adds to the limited studies on microchannel condensers with the extraction design. The extraction is designed to happen in one of the intermediate headers. Our objective is to provide a theoretical basis for the improvement of microchannel condensers by liquid extraction. Using an experimentally validated model, the effect of separation efficiency on the condenser performance is studied on a microchannel condenser that is tested in experiments.

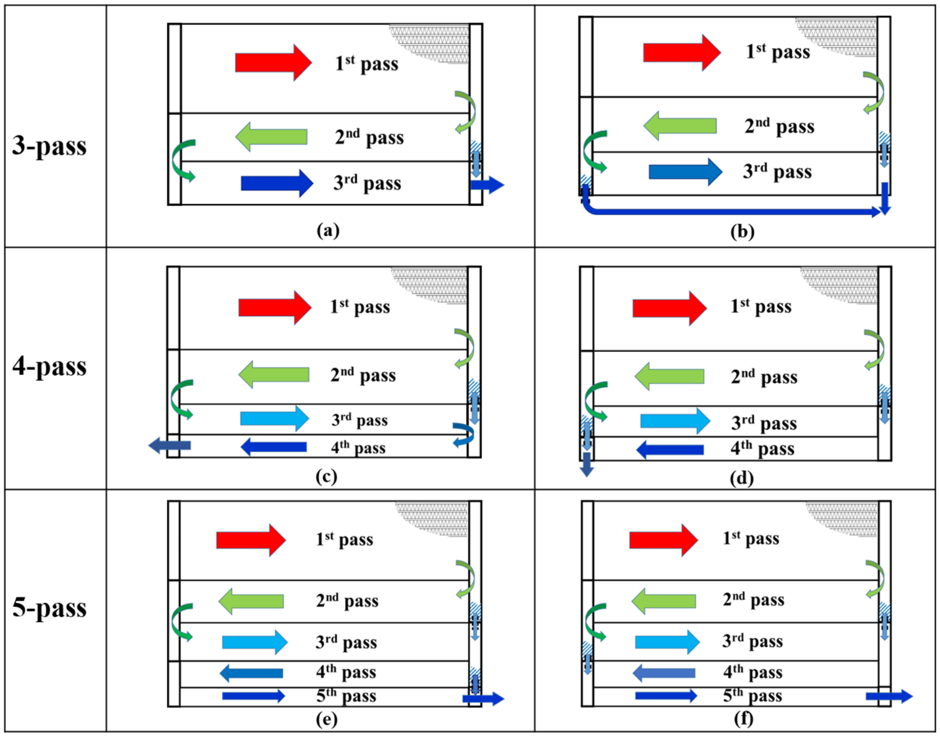

Figure 1: Some possible circuitries for extraction condensers

2. DESCRIPTION OF THE CONDENSER

A 4-pass conventional microchannel condenser from by a major heat exchanger manufacturer for mobile air conditioning systems is selected in the present study. The corresponding extraction design is the same circuitry as Figure 1(c): liquid is extracted from the second header at the outlet of the 1st pass.

Figure 2 shows the condenser that has been modified to be able to run in two modes: the conventional mode and the extraction mode. In Figure 2(a), instead of punching a hole in the lower baffle of the second header, a bypass transparent tube (extraction tube) for the 2nd and the 3rd pass is installed to simulate the extraction hole – this extraction design is named the single extraction tube. A needle valve is installed on the extraction tube to simulate various sizes of the extraction hole. When the needle valve is shut, the flow rate in the extraction path will be zero; the condenser is in the conventional mode. When the needle valve is open, the extraction tube allows a certain flow rate to be drained out of the second header. The flow coming out of the 3rd pass will recombine with the extracted flow at the inlet to the 4th pass. A Coriolis-type mass flow meter is installed on the extraction tube to measure the flow rate provided that the extracted flow is in single phase.

The needle valve is chosen from a major valve manufacturing company for 1/4” tubes. The extraction tube is chosen to be 1/4” transparent PFA tube with 1/8” inner diameter, with a total length of 2200 mm. The sizes of the needle valve and extraction tube are chosen based on 1) the pressure drop balance between the flows in the extraction tube and the 2nd-3rd passes; 2) the maximum opening allows the highest liquid flow rate from the second header to flow through at several nominal conditions.

To compare with the single extraction tube, a double-extraction-tube design shown in Figure 2(b) is also studied numerically. The advantage of double extraction tubes is to quantify the extracted two-phase flow from the second header. In Figure 2(b), the extracted flow first comes across an impacting T-junction separator, in which liquid and vapor separate from each other completely. The T-junction tube separates the flow into two extraction tubes: the vapor extraction tube and the liquid extraction tube, therefore, this design is named double extraction tubes. The flow rate for each phase is then measured by a mass flow meter downstream, respectively. Downstream of the mass flow meter on each extraction tube, a needle valve is also installed to simulate the size of the extraction hole. The diameter of the

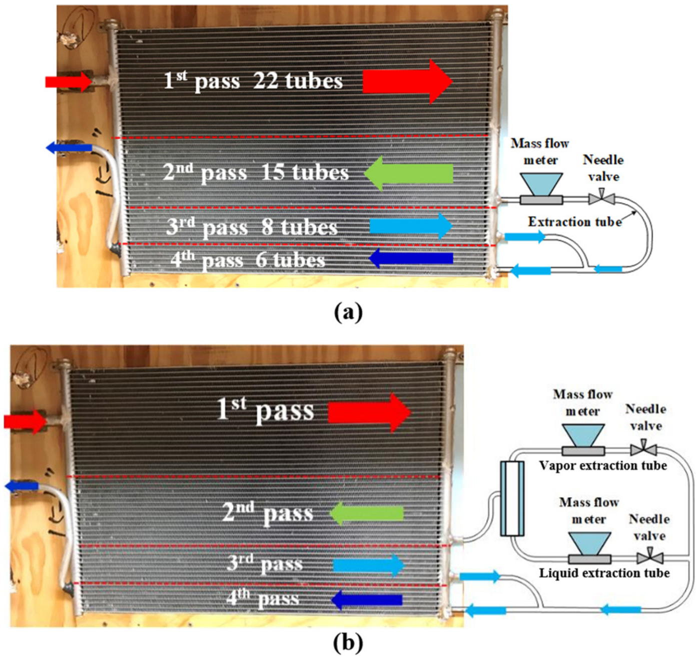

Figure 2: Condenser modified to run in both the conventional mode and the extraction mode: (a) single-extraction-tube design; (b) double-extraction-tube design

liquid extraction tube and the model of the valve on it are selected to be the same as those for the single-extraction-tube design. The maximum cross-section area of the flow passage of double extraction tubes is theoretically larger than the single extraction tube – we will investigate the difference this will cause to the characteristics of flow extraction.

Table 1 presents the main geometrical dimensions of the condenser. The microchannel port in one microchannel tube is estimated to have a hydraulic diameter of 0.67 mm. The number of microchannel ports per tube is 16. The fin density of the condenser is 17 per inch, the face area 0.2447 m^2, the total air-side area 5.2895 m^2, and the total refrigerant-side area 1.3232 m^2.

Table 1: Main geometrical dimensions of the microchannel condenser in Figure 2

Item	Value	Item	Value
Width w. headers [mm]	620	Louver pitch [mm]	0.77
Width w/o headers [mm]	590	Louver length [mm]	6.0
Width covered by fin [mm]	575	Louver angle [-]	27
Height w/ side plates [mm]	405	Header type	D-shape
Height w/o side plates [mm]	390	Header equivalent diameter [mm]	18.0
Depth [mm]	16.0	Length of the extraction tube [mm]	2200
MC tube thickness [mm]	1.0	Diameter of the extraction tube [mm]	3.175
MC tube pitch [mm]	7.8	Length of the vapor extraction tube [mm]	2400
MC port D_h [mm]	0.67	Diameter of the vapor extraction tube [mm]	6.35
Number of MC ports per tube [-]	16	Length of the liquid extraction tube [mm]	2550
Fin thickness [mm]	0.1	Diameter of the liquid extraction tube [mm]	3.175
Fin pitch [mm]	1.53		

3. MODEL DESCRIPTION

Park and Hrnjak (2008) built a conventional microchannel condenser model for steady-state operation using 1-D finite-volume discretization. We adopt the same methodology in the present study to model our extraction condenser. In the model, the following assumptions are made for one pass of the microchannel condenser: (1) Refrigerant distribution is uniform among microchannel tubes (maldistribution has less effect in condensers than in evaporators); (2) at each port in the same tube, the refrigerant mass flow rate is the same; (3) no heat is conducted along the tube nor between tubes through fins; (4) all headers are adiabatic; (5) incoming air has a uniform temperature and velocity profile.

The empirical correlations for heat transfer and pressure drop are listed in Table 2. The heat transfer correlation for the condensing superheated region can be referred to (Xiao and Hrnjak, 2017). On the air side, the condition for determining the heat transfer coefficient is the inlet condition, so the heat transfer coefficient is calculated as a constant due to uniform air inlet velocity and inlet temperature. The refrigerant properties are calculated by REFPROP 10.0 (Lemmon et al., 2018) and the simulation is carried out in MATLAB 2018a.

Figure 3 shows nomenclature for quantification of the liquid and vapor extraction in the second header. Two efficiencies are defined for liquid and vapor, respectively. The liquid extraction efficiency, η_L, is defined as the ratio of the liquid mass flow rate through the extraction hole to the total liquid mass flow rate coming into the header, as shown by Eq. (1). The vapor separation efficiency, η_V, is evaluated as the ratio of the vapor mass flow rate going into the downstream pass to the total vapor mass flow rate entering the header, as shown by Eq. (2).

$$\eta_L = \frac{\dot{m}_{L,extrac}}{\dot{m}_{L,extrac} + \dot{m}_{2Li}} \tag{1}$$

Table 2: Summary of heat transfer and pressure drop correlations

Item	Correlation
Air side	
Heat transfer coefficient	Chang and Wang (1997)
Pressure drop	Chang and Wang (1996)
Refrigerant side – Single-phase region	
Heat transfer coefficient	Gnielinski (1976)
Frictional pressure drop	Churchill (1977)
Refrigerant side – Two-phase region	
Heat transfer coefficient	Cavallini *et al.* (2006)
Frictional pressure drop	Cavallini *et al.* (2006)
Deceleration pressure drop	Cavallini *et al.* (2009)
Refrigerant side – Condensing superheated region	
Heat transfer coefficient	Xiao and Hrnjak (2017)

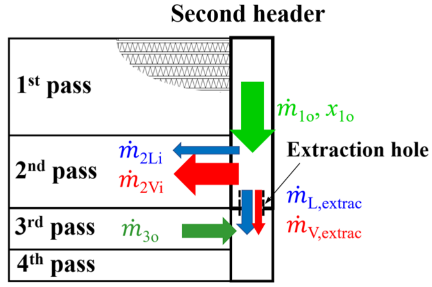

Figure 3: Parameters related to the definition of separation efficiencies of the extraction header

$$\eta_{\mathrm{V}} = \frac{\dot{m}_{\mathrm{2Vi}}}{\dot{m}_{\mathrm{2Vi}} + \dot{m}_{\mathrm{V,extrac}}} \tag{2}$$

where $\dot{m}_{\mathrm{V,extrac}}$ and $\dot{m}_{\mathrm{L,extrac}}$ are the vapor mass flow rate and liquid mass flow rate extracted through the extraction hole; $\dot{m}_{\mathrm{2Vi}}$ and $\dot{m}_{\mathrm{2Li}}$ are the vapor mass flow rate and liquid mass flow rate at the inlet of the 2nd pass. The range for both η_{L} and η_{V} is [0, 1].

In the extraction condenser shown in Figure 1(c), there is a governing equation denoting that the pressure drop in the 2nd and the 3rd passes ($\Delta P_{2\text{-}3}$) is equal to the pressure drop in the extraction hole. For the two designs in Figure 2, the pressure drop in the 2nd and the 3rd passes is equal to the pressure drop in one extraction tube. The schematics of flow resistance network for those two designs are shown in Figure 4. While the flow resistance of the only one extraction tube in Figure 4(a) is regulatable, the flow resistances of both extraction tubes in Figure 4(b) are regulatable. That is because when a certain $\dot{m}_{\mathrm{L,extrac}}$ goes through the liquid extraction tube at a certain valve opening, the pressure drop in the liquid extraction tube is fixed. While $\dot{m}_{\mathrm{2Li}}$ can be calculated by

$$\dot{m}_{\mathrm{2Li}} = \dot{m}_{\mathrm{1o}} \cdot \left(1 - x_{\mathrm{1o}}\right) - \dot{m}_{\mathrm{L,extrac}} \tag{3}$$

$\dot{m}_{\mathrm{2Vi}}$ has to be fixed to match $\Delta P_{2\text{-}3}$ with the pressure drop in the liquid extraction tube. Then, $\dot{m}_{\mathrm{V,extrac}}$ also has to be fixed based on

$$\dot{m}_{\mathrm{V,extrac}} = \dot{m}_{\mathrm{1o}} \cdot x_{\mathrm{1o}} - \dot{m}_{\mathrm{2Vi}} \tag{4}$$

Therefore, the flow resistance of the vapor extraction tube has to be regulated to match the pressure drop in it with $\Delta P_{2\text{-}3}$. This is why both extraction tubes Figure 4(b) need to have a needle valve to regulate the flow inside.

4. RESULTS AND DISCUSSION

4.1 Experimental validation of the model

Experiments for the single-extraction-tube design in Figure 2(b) are conducted on a mobile air conditioning test facility. It was introduced in Li and Hrnjak (2017a). The condenser model is validated by experimental data under operating conditions per SAE Standard J2765 (SAE International, 2008). The working fluid is R134a. The compressor uses PAG 46 synthetic oil. In experiments, 50 conditions are run in the conventional mode and 39 conditions are run in the extraction mode. The air inlet temperature is set to be 35 ºC, 40 ºC, or 45 ºC. The air face velocity is in the range of 1.6 – 3.7 m/s. The R134a-oil inlet pressure (P_{cmi}) ranges from 1283.4 to 1858.1 kPa, and the R134a-oil mass flow rate ($\dot{m}_{\mathrm{m}}$) from 24.3 to 46.0 $\mathrm{g \cdot s^{-1}}$, which corresponds to mass flux through the 1st pass in the range of 195 – 368 kg/($\mathrm{m^2}$-s). The OCR ranges from 0.04 – 0.07. The subcooling at the condenser exit is controlled in the range of 0 – 22.6 K.

For model validation for the extraction mode, $\dot{m}_{\mathrm{1o}}$ in Figure 3 is equal to refrigerant mass flow rate $\dot{m}_{\mathrm{r}}$ and is measured in the system; x_{1o} in Figure 3 is calculated by the model. Besides them, either η_{L} or η_{V} shown in Figure 3 must be an

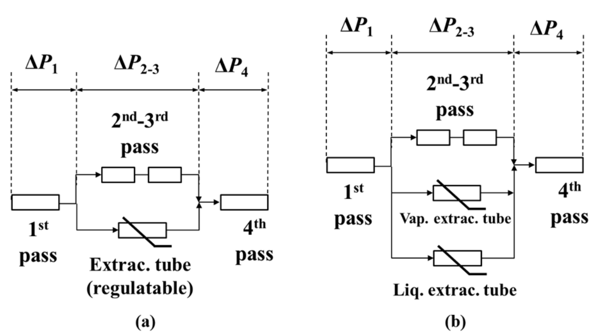

Figure 4: Flow resistance network of the extraction condenser: (a) single-extraction-tube design; (b) double-extraction-tube design

input to the model to fix the condenser working state. It has been found from our experiments that when the valve opening in Figure 2(a) is very small, the flow in the extraction tube is in single phase. Then, $\dot{m}_{L,extrac}$ in Eq. (1) can measured and η_L can thus be deducted. If the valve opening in Figure 2(a) is not very small, it is found from the experiments that the flow in the extraction tube is two-phase, but η_V is found by modeling to vary in much smaller range than η_L (details in *4.2 Single extraction tube*). Therefore, we assume η_V to be the median value of its plausible range when the flow in the extraction tube is two-phase.

Figure 5 shows the comparison between the experimental results and the modeling results for the heating capacity Q_c and the pressure drop ΔP_c of the condenser in both the extraction mode and the conventional mode. Figure 5(a) shows the comparison of predicted and measured Q_c. 80 % of the data points are predicted within +/-5 % deviation from the experimental results. Figure 5(b) compares the predicted and measured ΔP_c. 83 % of the data points are predicted within ±25 % deviation from the experimental results. Overall, the modeling results show good agreement with the experimental results.

Not only the pressure drop for the whole condenser is measured, the pressure drop in the 1st pass and the first three passes are also measured. Figure 6(a) compares the experimental results and the modeling results for the pressure drop in the 1st pass, ΔP_1. 76 % of the data points are predicted within +/-25 % deviation from the experimental results. Figure 6(b) compares the experimental results and the modeling results for the pressure drop in the first three passes, $\Delta P_{1\text{-}3}$. 76 % of the data points are predicted within ±25 % deviation from the experimental results. The modeling results for the pressure drop in individual passes are about as accurate as those for the pressure drop in the whole condenser.

4.2 Results for the single-extraction-tube design and the double-extraction-tube design

Following the experimental validation, the single-extraction-tube design in Figure 2(a) is studied first by the model. An R134a operating condition is chosen from the experimental data for the conventional mode in Figure 5. All parameters of this operating condition are inlet parameters, and they are listed in Table 3.

In Figure 7(a), the condenser model outputs a curve of η_V a function of η_L for each needle valve opening (one C_v value denotes one valve opening) on the extraction tube – here we assume η_L can vary arbitrarily. These results in Figure 7(a) are only based on the pressure drop balance between the extraction tube and the 2nd-3rd passes. Theoretically, a second header model will calculate the real value of η_L. In the second header, η_L is determined by the header geometry, two-phase fluid dynamics, and pressure boundary conditions. The second header model will be built in our future work.

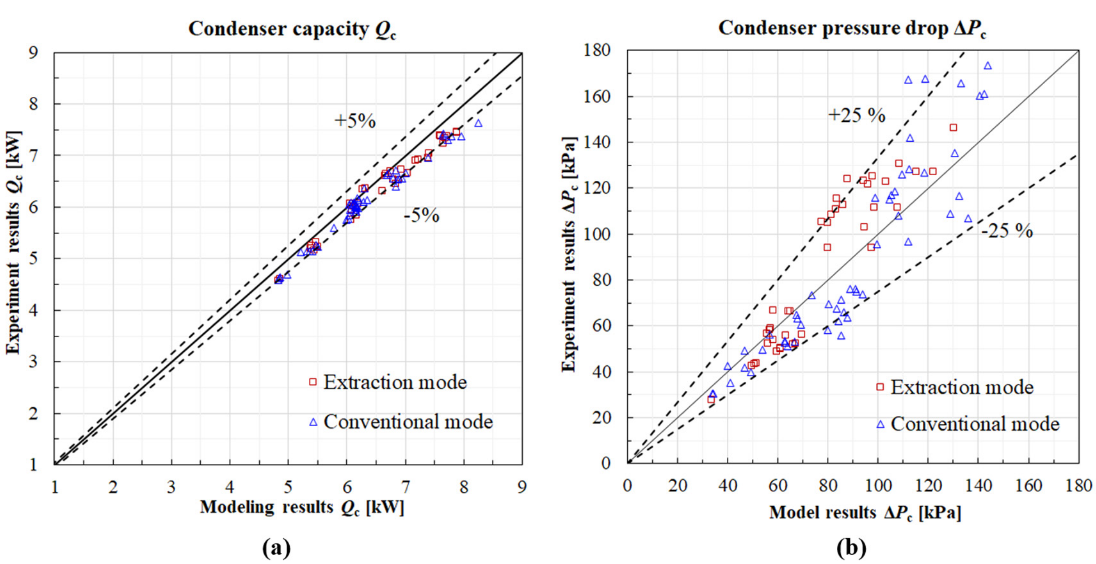

Figure 5: Comparison of the experiment results and the model results: (a) condenser capacity; (b) condenser pressure drop

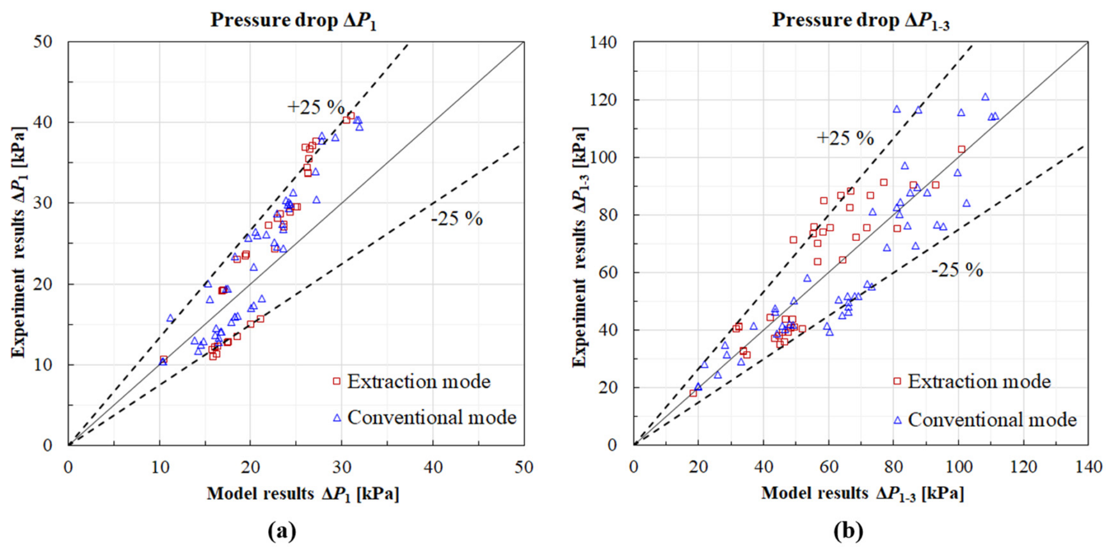

Figure 6: Comparison of the experiment results and the model results: (a) refrigerant pressure drop in the 1st pass; (b) refrigerant pressure drop in the 1st pass to the 3rd pass

Table 3 R134a operating condition for the simulation

Parameter	Value
$\dot{m}_r$ [g/s]	36.6
P_{cri} [kPa]	1493.6
T_{cri} [°C]	86.0
T_{cai} [°C]	35.3
v_{cai} [m s^{-1}]	2.00
RH_{cai} [-]	16.9 %

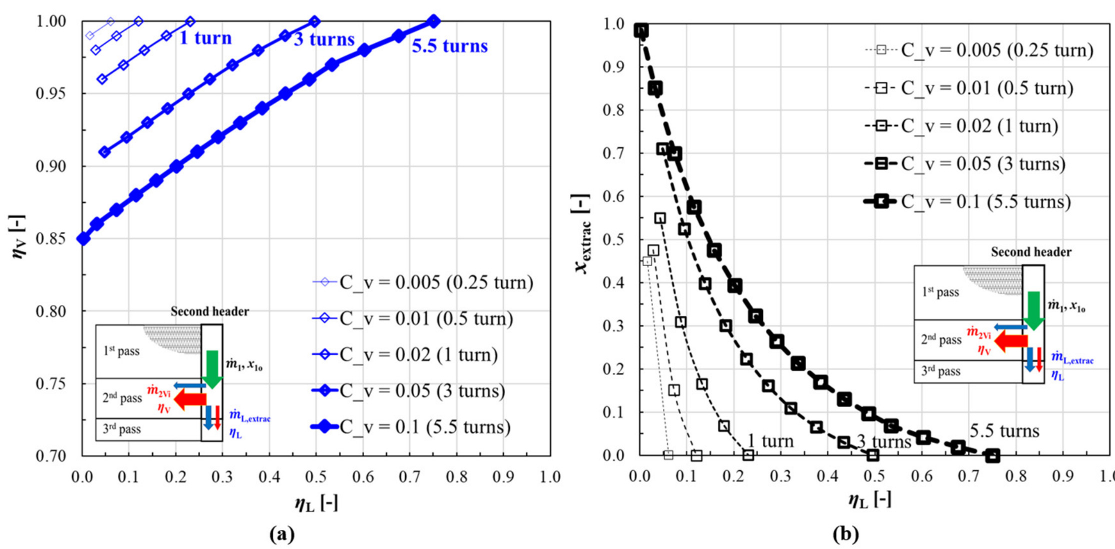

Figure 7: Flow characteristics for the single-extraction-tube design: (a) η_V as a function of η_L; (b) x_{extrac} as a function of η_L (inlet condition in Table 3)

Figure 7(a) shows η_V increases monotonically as η_L increases. When a higher $\dot{m}_{L,extrac}$ is extracted from the second header (η_L increases), ΔP in the extraction tube will increase and $\dot{m}_{2Li}$ will decrease based on Eq. (3), so $\dot{m}_{2Vi}$ has to increase (η_V increases) so that $\Delta P_{2\text{-}3}$ equals to ΔP in the extraction tube.

It is only physically possible for η_L to be in a certain range within [0, 1]. Taking C_v = 0.1 (5.5 turns) for the valve as an example, η_L starts from 0 and ends at 0.75, because when η_L is higher than 0.75 ΔP in the extraction tube will be too large for $\Delta P_{2\text{-}3}$ to match. When the condenser geometry or the operating condition changes, the physical range for η_L will change. It is worth noting that, as a function of η_L, the physically plausible range of η_V is [0.85, 1], which is only on the higher end of its whole range [0, 1]. When η_V is lower than 0.85, more than 15 % of the vapor flow rate goes into the extraction tube, ΔP in the extraction tube will be too large for $\Delta P_{2\text{-}3}$ to match even though all the liquid flow rate goes into the 2nd pass (η_L = 0).

Figure 7(a) also presents the difference in the separation phenomena among the five openings of the needle valve. The extraction tube with a larger C_v has a larger cross-sectional area, thus allowing a higher $\dot{m}_{V,extrac}$ at the same value of η_L. Therefore, η_V becomes smaller, i.e., the η_V-η_L curve is shifted downward. Meanwhile, the physically plausible range for η_L becomes larger with a larger C_v. It worth noting that the smallest valve opening: C_v = 0.005, the physically plausible range for η_L is [0.016, 0.061], which is very small, and the corresponding range for η_V is also very small: [0.99, 1].

For the same conditions in Figure 7(a), Figure 7(b) shows that x_{extrac} reduces as η_L increases. This is because as $\dot{m}_{L,extrac}$ increases, $\dot{m}_{2Vi}$ increases and $\dot{m}_{V,extrac}$ decreases, therefore, x_{extrac} reduces. In addition, the slope of the x_{extrac} - η_L curve depends on C_v and becomes larger in magnitude as C_v becomes smaller. In other words, x_{extrac} changes more dramatically as a function of η_L at a smaller valve opening. For example, at the smallest C_v (0.005), x_{extrac} reduces from 0.45 to 0 as η_L changes from 0.016 to 0.061.

Figure 8(a) and (b) show the capacity Q_c and ΔP_c for the condenser, respectively. Based on the criterion to compare condensers which is used in Li and Hrnjak (2021b): at the same air and refrigerant inlet conditions, the condenser with a bigger Q_c is more effective. In Figure 8(a), for one valve opening, Q_c increases monotonically as η_L increases. The highest Q_c (6974.2 W) happens at C_v = 0.05, η_L = 0.50. Similar to the curves for $\dot{m}_{extrac}$ and x_{extrac}, Q_c increases the most (57.2 W) at the largest opening (C_v = 0.1). Figure 8(b) shows that the smallest valve opening causes the largest ΔP_c, which is intuitive because the flow resistance of the condenser becomes bigger as valve opening decreases. For the openings of 5.5 turns and 3 turns, there is a η_L value which cause the largest ΔP_c, whereas for the other openings ΔP_c increases as η_L increases. Yet, the change for each opening stay within 3 % of the lowest ΔP_c for that opening.

Finally, Figure 9(a) shows η_V increases monotonically as η_L increases for the double-extraction-tube design for the

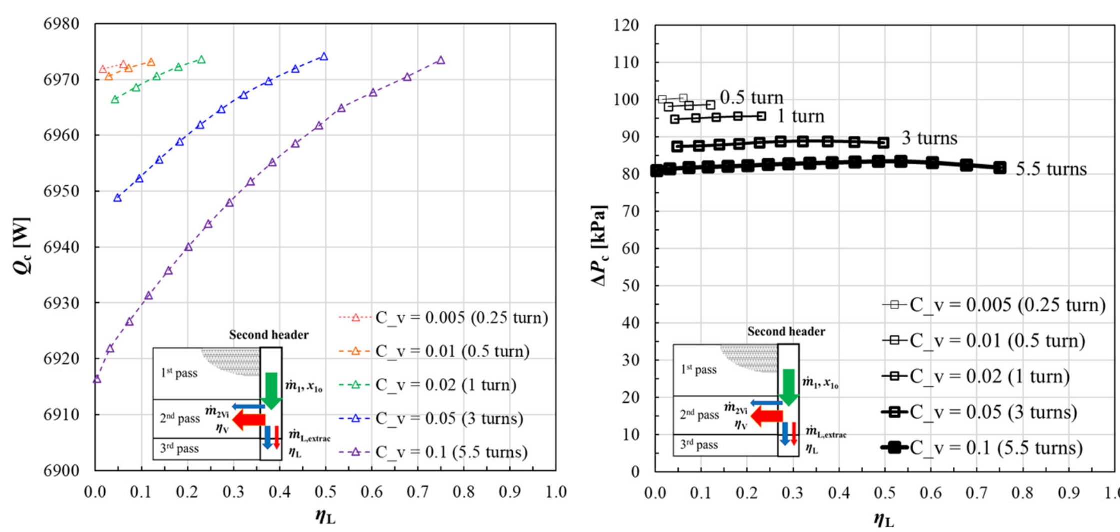

(a) (b)

Figure 8: Condenser working performance as function of η_L for the single-extraction-tube design: (a) Q_c; (b) ΔP_c (inlet condition in Table 3)

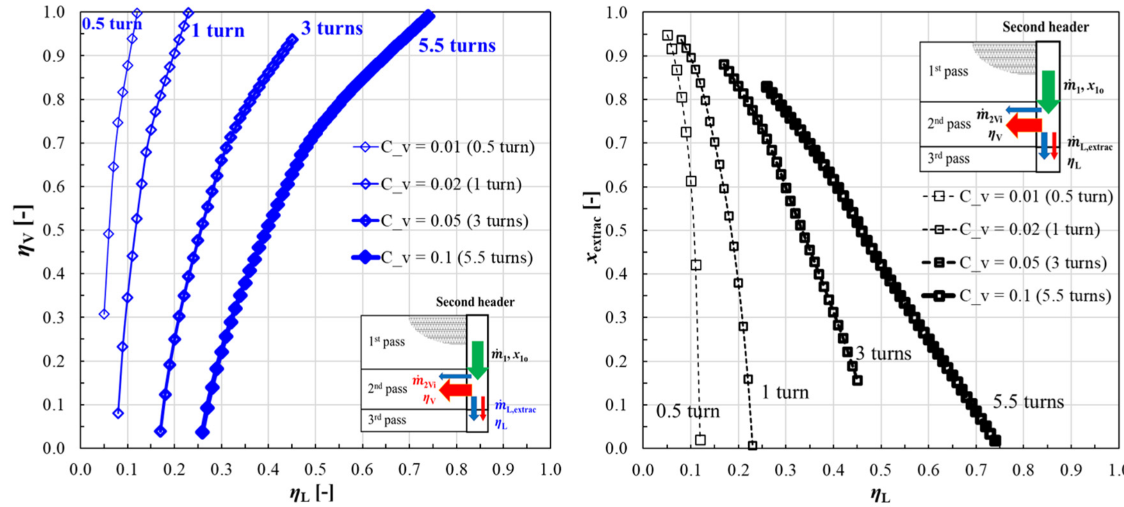

(a) **(b)**

Figure 9: Flow characteristics for the double-extraction-tube design: (a) η_V as a function of η_L; (b) x_{extrac} as a function of η_L (inlet condition in Table 3)

same inlet condition in Figure 7. Compared to the range of η_V in Figure 7(a), the range of physically plausible η_L becomes smaller and the range of of η_V in Figure 9(a) becomes much larger. This is because the pure liquid goes into the liquid extraction tube. $\dot{m}_{L,extrac}$ cannot be too low then the pressure drop in the liquid extraction tube will be too low. On the other hand, $\dot{m}_{2Vi}$ can be very low because of the low pressure drop in the liquid extraction tube. Similar to Figure 7(b), Figure 9(b) shows that x_{extrac} reduces as η_L increases for the double-extraction-tube design.

4. SUMMARY AND CONCLUSION

This study presents the flow characteristics in a microchannel condenser with flow from the second header. The condenser is modified to be able to run in both the extraction mode and the conventional mode for comparison. A 1-D numerical model is built to predict the performance of the condenser in both modes and validated with the experimental data. Most of the data for the capacity agree within ±5 % and most of the data for the pressure drop agree within ± 25 %.

It is found that without an interior separator complete separation in the second header is almost impossible. Based on the pressure drop balance between the extraction tube and the 2nd-3rd passes, a physically possible range of η_L is calculated by the model. A larger opening of the needle valve allows a larger range for η_L. η_V increases monotonically as η_L increases. Compared to the single-extraction-tube design, the double-extraction-tube design allows a smaller range of η_L and a much larger range for η_V. The extracted quality decreases as η_L increases. The condenser capacity increases as η_L increases. The experimental comparison between the two modes is in a companion paper.

NOMENCLATURE

ΔP	pressure drop	(kPa)
$\dot{m}$	mass flow rate	(g/s)
OCR	oil circulation ratio	(-)
P	pressure / pitch	(kPa) / (mm)
Q	capacity	(kW)
RH	relative humidity	(-)
T	temperature	(°C)
UA	thermal conductance	(W/K)
v	velocity	(m/s)
x	vapor quality	(-)

Greeks

η	separation efficiency	(-)
ρ	density	(kg/m^3)

Subscripts

1-3	1st pass to 3rd pass
1o	1st pass outlet
2Vi	2nd pass vapor inlet
2Li	2nd pass liquid inlet
3o	3rd pass outlet
c	condenser
ca	condenser air side
cai	condenser air inlet
cmi	condenser mixture inlet
L	liquid
m	refrigerant-oil mixture
r	refrigerant
V	vapor

REFERENCES

Chen, Y., Hua, N., Deng, L. S. 2012. Performances of a split-type air conditioner employing a condenser with liquid–vapor separation baffles. Int. J. Refrig. 35(2), 278-289.

Li, J., Hrnjak, P., 2017a. Improvement of condenser performance by phase separation confirmed experimentally and by modeling. Int. J. Refrig. 78, 60-69.

Li, J., Hrnjak, P., 2017b. Separation in condensers as a way to improve efficiency. Int. J. Refrig. 79, 1-9.

Li, J., Hrnjak, P., 2021a. An experimentally validated model for microchannel condensers with separation circuitry. Appl. Therm. Eng., 183, 116114.

Li, J., Hrnjak, P., 2021b. Optimization of a microchannel condenser with separation circuitry. Appl. Therm. Eng., 184, 116273.

Li, J., Hu, S., Yang, F., Duan, Y., Yang, Z., 2019. Thermo-economic performance evaluation of emerging liquid-separated condensation method in single-pressure and dual-pressure evaporation organic Rankine cycle systems. Applied Energy, 256, 113974.

Luo, X, Yi, Z, Chen, Z, Chen, Y, Mo, S., 2016. Performance comparison of the liquid–vapor separation, parallel flow, and serpentine condensers in the organic Rankine cycle. Applied Therm. Eng. 94, 435-48.

SAE International, 2008. Procedure for Measuring System COP [Coefficient of Performance] of a Mobile Air Conditioning System on a Test Bench, SAE Surface Vehicle Standard J2765 OCT2008.

Park, C.Y., Hrnjak, P., 2008. Experimental and numerical study on microchannel and round-tube condensers in a R410A residential air-conditioning system. Int. J. Refrig. 31(5), 822-831.

ACKNOWLEDGMENT

The authors thankfully acknowledge the financial and technical support provided by the Air Conditioning and Refrigeration Center at the University of Illinois at Urbana-Champaign and Creative Thermal Solutions, Inc.